Probing the beam-induced heating effect inside a transmission electron microscope by nanoparticle labels

Lei Zhang
Southest University
Longbing He
Southeast University
Yufeng Yang
Southeast University
Hua Hong
Southeast University
Luping Tang
Southeast University
Litao Sun (slt@seu.edu.cn)
SEU-FEI Nano-Pico Center

Nano Express

Keywords: Transmission Electron microscopy; Heating effect; Nanoparticle; Temperature gradient

Posted Date: February 6th, 2020

DOI: https://doi.org/10.21203/rs.2.22801/v1

Version of Record: A version of this preprint was published at Micro & Nano Letters on April 20th, 2021.
See the published version at https://doi.org/10.1049/mna2.12049.

Abstract

Beam-induced heating effect on nanoscale samples is a crucial question as it strongly influences the interpretation of observed unusual behaviors. This question is currently under debate without a convincing conclusion. Here, using silver nitride (Ag 3 N) nanoparticles as temperature labels, we perform an investigation on this heating effect inside a transmission electron microscope (TEM) under normal imaging conditions. Combined with experimental measurements and semi-quantitative calculations, a temperature increase of more than 100 K is estimated and confirmed in the graphite carbon nitride (g-C 3 N 4) films. Strong temperature gradients are found to exist in the single-end fixed g-C 3 N 4 films. The influencing factors of heat accumulation are also investigated and discussed. Findings in this paper may shed some light on the understanding of the abnormal behaviors of nano-objects observed inside TEM.

1. Introduction

Transmission electron microscope (TEM) is one of the most powerful equipment used to characterize materials for their structures, phases, compositions, and properties. The elastic or inelastic interactions between high-energy electrons and specimen atoms enable precise determination of atom arrangements and elemental distributions, providing deep insight into the material structures and related properties. In terms of these interactions, significant side-effects usually co-occur during TEM observation and imaging, including sputtering [1], amorphization [2], ionization [3], carbonization [4], local heating [5], etc. Among all these side-effects, the electron-beam induced local heating is quite elusive as it is currently neither able to directly measure the precise temperature increase inside the local nanometer-sized specimen nor able to quantitatively determine how much energy has been transformed into heat and kept inside the specimen. Although there are ways to minimize the beam-heating effect, e.g. using a quite low-dose beam to image together with a substrate with very high thermal conductivity, beam-induced abnormal phenomena are still frequently observed on nanometer-sized objects during imaging [5–7]. It reflects that the local heating effect may hardly be avoided in many cases. Thereby, a temperature increase could exist and bring considerable interference in understanding the intrinsic properties of the samples from the observed unusual behaviors, especially for metastable and low-dimension functional materials [8, 9]. As early as in 1980s, Iijima et al showed that Au nanoparticles deposited on a carbon substrate could be excited during TEM observation [10]. The geometric shapes of the Au nanoparticles fluctuated frequently when they were irradiated by the electron beam. This phenomenon was identified as quasi-melting and further similar experiments demonstrated that the electron-beam induced temperature effect was a key reason accounting for the phenomenon. Aside from such notable shape changes, the temperature effect is also very often doubted to play a role in many other behaviors observed in TEM, e.g. the abnormal deformation behaviors of nanoscale metals, semiconductors and oxides [11], the phase transitions in nanowires and nano-belts [12], the reconstruction and recrystallizations in amorphous nanoparticles [13, 14].

Generally, the electron-beam induced temperature increase mainly depends on two aspects, that is, the used beam intensity and voltage which govern the input energy to the specimen, and the supporting

substrate which determines the heat dissipation. Li et al estimated that an electron beam having energy between 500 eV and 2 keV could cause a temperature rise up to a few hundred degrees on an organic specimen [15]. Egerton et al indicated that materials with low thermal conductivity (e.g. 0.2-2 W/mK) could be melted or thermally degraded even under a relatively low beam density [16]. Yokota et al found that AlSi nanoalloys could be easily melted during TEM imaging due to electron thermal spikes in the particles and poor thermal conduction away from the particles [17]. In a recent study, Asoro et al reported that even for metal nanoparticles supported on carbon films, a temperature increase of 58 K was estimated to be induced by the electron beam during normal imaging [18]. All these investigations imply that the temperature effect during TEM imaging is somehow inevitable. Unfortunately, from current studies, it is hard to make a conclusion on how severe the temperature effect is and what influence will appear subsequently. As a result, the temperature effect is often argued in the interpretations of new phenomena observed in TEM but usually without a convincing conclusion.

In order to probe into this question, we here perform an in-situ investigation using Ag_3N-decorated-g-C_3N_4 samples as a model. The decomposition of the Ag_3N nanoparticles can serve as temperature labels, providing a direct profile of the temperature distribution in the g-C_3N_4 film induced by electron irradiation.

2. Experimental

Materials preparation

Ag_3N nanoparticles were synthesized by dissolving silver nitrate ($AgNO_3$) in concentrated ammonia solution [19, 20]. Typically, 0.25 g $AgNO_3$ was added into 50 ml deionized water and magnetically stirred for 30 min to form the $AgNO_3$ solution. Then, a 50 ml sodium hydroxide (NaOH) solution (0.1M) was added to the $AgNO_3$ solution dropwise. The amount of NaOH was superfluous and thus silver oxide (Ag_2O) nanoparticles precipitated during the reaction. After the reaction, the turbid liquid was centrifuged and washed to obtain Ag_2O particles. Ag_3N nanoparticles were acquired by adding the Ag_2O particles into superfluous ammonia water. The g-C_3N_4 films were bought from Aladdin Company. Ag_3N-decorated-g-C_3N_4 samples were obtained by mixing the Ag_3N nanoparticles with g-C_3N_4 films in an ammonia solution.

TEM characterization and in-situ heating

A 300 kV TEM (FEI, Titan) was used to conduct the experiment with a beam intensity of 1.6×10^4 A/m^2. The temperatures at which Ag_3N nanoparticles decomposed were calibrated using a heating holder (Protochips Aduro™) with electrical chip (E-chip). The E-chip contained hole-arrays as observation windows, and holey carbon films were overlaid on the windows to support the nano-specimens. By controlling the applied current, the heating temperature of the E-chip can be precisely programmed. As the nominal ramp rate of the E-chip is 1000 K/ms, the retardation of the temperature increase during heating can thus be neglected [21].

3. Results And Discussion

Figure 1a shows the topography of a typical Ag_3N-decorated-g-C_3N_4 sample. Figure 1b shows the energy dispersive X-ray (EDX) spectrum of the film. The strong peaks of carbon (C) and nitrogen (N) elements demonstrate the integrality of the g-C_3N_4 film. Notably, C signal is influenced by other sources such as the supporting substrate, so the signal ratio of C to N elements varies and can not represent the component proportion of the g-C_3N_4 film. Figure 1c shows a high-resolution TEM image of a Ag_3N nanoparticle. From the fast Fourier transform pattern shown in Fig. 1d, the crystalline structure of Ag_3N can be identified and confirmed by the (0–2 2), (2–2 2) and (2 0 0) planes [22], with zone axis [0 1 1].

It is observed that the Ag_3N nanoparticles on the g-C_3N_4 film cannot sustain long time TEM imaging. Under a beam intensity of 1.6×10^4 A/m^2, decomposition of the Ag_3N nanoparticles gradually occurs. Figures 2a-2j show a typical decomposition process of the Ag_3N nanoparticles with diverse sizes. As can be seen, several Ag_3N nanoparticles start to decompose much earlier and faster than the others. However, all the Ag_3N nanoparticles vanish eventually under continuous irradiation, leaving only the g-C_3N_4 frames. These asynchronous decomposition processes imply that the electron beam induced heat accumulation is uneven in the g-C_3N_4 film. Thereby, the sequence of the vanishing process of the Ag_3N nanoparticles gives direct information of the distribution of the beam induced heating effect.

To facilitate checking the heat distribution, eight Ag_3N nanoparticles are selected and their shape evolutions are recorded by measuring their projection areas from the TEM image sequence. Figure 3 collects their projection areas as a function of irradiation time. Most Ag_3N nanoparticles present two stages before totally vanishing. In the first stage, their shapes change a little during the initial irradiation, possibly due to the shape/structural relaxation of the initial metastable states. In the second stage, continuous size reduction appears, indicating the start of structural decomposition induced by strong heat accumulation. Notably, nanoparticles marked by 1 and 5 which are located at the edge present a much earlier start of decomposition than the others. Their absence of the first stage implies that the beam induced heating effect on nanoparticles located at the film edge is much more severe due to the weak heat dissipation into surroundings. Statistical data prove that the decomposition of Ag_3N nanoparticles is dominated by the beam induced heating effect but not the beam sputtering.

Bulk Ag_3N is known to decompose at a temperature around 400 K [23]. However, the decomposition temperature of Ag_3N nanoparticles may change due to size effect [24]. To verify the decomposition temperature of the Ag_3N nanoparticles, a heating holder was used to carry out a calibration.Holey carbon films are applied as supporting substrate instead of g-C_3N_4 films as they have a much higher thermal conductivity and this can be helpful to relieve thermal retardation. Using the same beam intensity of 1.6×10^4A/m^2, it is found that the Ag_3N nanoparticles can sustain a heating temperature below 380K. When the heating temperature is increased to above 380K, the Ag_3N nanoparticles start to decompose. In order to double check the accuracy of the heating e-chip, bismuth (Bi) nanoparticles are used to make a

comparison. The temperature from the heating e-chip is verified and the mean decomposition temperature of the Ag_3N nanoparticles is thus estimated as 380K. (see details in Supplementary).

A method developed by Liu and Risbud is employed to semi-quantitatively calculate the heat accumulation during electron beam irradiation by treating the system as spherical particles embedded in thin films [25]. The input power is generated from electron collisions considered as cylindrical thermal spikes [26, 27], and the heat dissipation is thermal conduction from the surrounding film. When the high energy electrons interact with the sample atoms, beam induced temperature increase can be modeled as

$$\Delta T = \frac{3JQ}{8ek} R_e^2 \ln\left(1 + \frac{4kt}{f\rho R_e^2}\right),$$

where J is the electron beam current density, e is the electron charge, k is the thermal conductivity of the surrounding film, R_e is the radius of area that electrons bombards on, t is the irradiation time, Q is the total energy loss of the electron, f and ρ is the heat capacity and mass density of particles, respectively. Briefly, Q can be divided into two parts, i.e. the electron excitation loss Q_e and the Coulomb encounter loss Q_c, which can be described as

$$Q_e = \frac{2\pi nZ^2 r_e^2 mc^2}{1837.5A\beta^2} \ln\left(\frac{T_m}{T_a}\right)$$

$$Q_c = \frac{2\pi nZr_e^2 mc^2}{\beta^2}\left[\ln\left(\frac{m^2c^4\beta^2}{Z^2I^2(1-\beta^2)}\right) - \beta^2 + 0.198\right]$$

n is the number density of atoms in the particle, Z is the atomic number, r_e is the classical electron radius, β is the ratio of accelerated electron and light speed, and IZ (= 13.54 eV) is the average ionization potential of the electrons in the atom. T_m and T_a can be described respectively as

$$T_m = (560.8/A)\frac{E}{mc^2}\left(\frac{E}{mc^2} + 2\right)$$

$$T_a = \frac{m}{M}\left(1 + Z^{2/3}\right)R_h$$

where E is the energy of electrons and R_h is Rydberg energy for hydrogen.

In order to make a direct comparison, Bi nanoparticles and holey carbon film are also considered in the calculation. It is important to note that, in the experiment, Bi nanoparticles located on the g-C_3N_4 film or holey carbon film as well as Ag_3N nanoparticles located on holey carbon film can remain well unchanged under the same irradiation condition described above. Figure 4a shows the calculated temperature increase ΔT during TEM imaging with a beam intensity of $1.6 \times 10^4 A/m^2$. Obviously, a heating-up of more than 100 K can be achieved when the substrate is g-C_3N_4 films (3.5 ± 0.3 W/mK [28]). In contrast, when holey carbon films are used as substrates (129 W/mK [29]), the temperature increase is only several kelvins. These results confirm that both the electron beam condition (acceleration voltage, beam intensity, irradiation time) and the substrate material play significant effects on the heat accumulation. As a result, Ag_3N nanoparticles located in the g-C_3N_4 films can decompose easily if heat cannot be dissipated timely. According to the calculation results, nanoparticles show a rapid temperature increase at first, and then the temperature increase becomes very sluggish. The rapidly upward region with several tens of seconds can well explain the existence of nearly stable stage (first stage) for particles inside the g-C_3N_4 network shown in Fig. 3. At this stage, the temperature increment is not high enough for nanoparticles to decompose. With further irradiation, nanoparticles finally get enough heat energy and decompose dramatically. The model is for the perfectly embedded nanoparticles those are in good contact with surroundings. In actual experiments, the various contact conditions between nanoparticles and surrounding films lead to the inconsistent start-point of decomposition. As for particles those are supported at the edge of film, the electron induced heat cannot be conducted through the surrounding film efficiently and the thermal conductivity used in above equation cannot be simply treated as the one of film network. Figure 4b gives the temperature increment of Ag_3N and Bi nanoparticles in network having different thermal conductivity after 180 s beam irradiation. The temperature increment is small enough and can be neglected when the thermal conductivity of film network are larger than 30 W/mK.

In order to estimate the heat dissipation from the supporting grid, a single-end fixed Ag_3N-decorated-g-C_3N_4 film was carefully examined. Figure 5 shows the illustration of the film sample with two monitored regions (red boxes). After 3-min irradiation with beam intensity of 1.6×10^4 A/m^2, the Ag_3N nanoparticles in the two regions show significant discrepancies. In the region nearby the supporting copper (Cu) grid, all the Ag_3N nanoparticles can well retain, even for the very small ones. In sharp contrast, the Ag_3N nanoparticles in the region which is far away from the supporting Cu grid largely vanish after beam irradiation. This evidence points out that a large temperature gradient should exist in the g-C_3N_4 film. The key factor causing this temperature gradient is the partially supported Cu grid. Therefore, during TEM imaging, the beam-induced temperature effect should be considered comprehensively, as the thermal conduction between nano-samples and supporting films as well as the thermal conductivity of the supporting film itself indeed plays crucial roles. Moreover, as for those large scale nanowires and membranes, significant thermal gradients may be induced during TEM imaging. This may cause usual behaviors that do not originate from their intrinsic properties.

4. Conclusions

Using Ag_3N nanoparticles as temperature labels, we have explored the temperature effect inside a TEM during normal imaging. The decomposition temperature of the Ag_3N nanoparticles is carefully calibrated to be 380 K by heating experiments. During normal imaging, a strong beam heating effect can be caused, and a semi-quantitative calculation indicates a temperature increase of more than 100 K in the g-C_3N_4 films due to heat accumulation, which well agrees with the experimental observation of Ag_3N nanoparticle decomposition during imaging. Significant temperature gradients are experimentally verified and demonstrated, possibly providing valuable information in understanding the unusual behaviors in nanomaterials.

Abbreviations

E-chip
Electrical chip
EDX
Energy Disperse X-ray
g-C_3N_4
graphite carbon nitride
TEM
Transmission Electron Microscopy

Declarations

Availability of Data and Materials

All data used within this work are available upon reasonable request.

Competing interests

The authors declare that they have no competing interests.

Funding

The research was supported by the National Key R&D Program of China Grant No. 2017YFA0403600 and the National Natural Science Foundation of China (Grant Nos. 51571060, 11774050, 51420105003, and 11525415).

Authors' contributions

ZL and HLB designed this work and performed the experiment with TEM. YYF prepared the materials. TLP and HH gave technical support and discussed the results. SLT supervised the projects. All authors read and approved the final manuscript.

Acknowledgments

Not applicable.

References

[1] Egerton RF, McLeod R, Wang F, Malac M (2010) Basic questions related to electron-induced sputtering in the TEM. Ultramicroscopy 110:991-997

[2] Li XB, Liu XQ, Liu X, Han D, Zhang Z, Han XD, Sun HB, Zhang SB (2011) Role of electronic excitation in the amorphization of Ge-Sb-Te alloys. Phys Rev Lett 107:015501

[3] Li A, Luo Q, Park SJ, Cooks RG (2014) Synthesis and catalytic reactions of nanoparticles formed by electrospray ionization of coinage metals. Angew Chem Int Edit 53:3147-3150

[4] Li Z, Lv W, Zhang C, Li B, Kang F, Yang QH (2015) A sheet-like porous carbon for high-rate supercapacitors produced by the carbonization of an eggplant. Carbon 92:11-14

[5] Shehla H, Ishaq A, Khan Y, Javed I, Saira R, Shahzad N, Maaza, M (2016) Ion beam irradiation-induced nano-welding of Ag nanowires. Micro Nano Lett 11:34-37

[6] Kryshtal AP, Minenkov AA, Ferreira PJ (2017) Interfacial kinetics in nanosized Au/Ge films: An in situ TEM study. Appl Surf Sci 409:343-349

[7] Guo H, Khan MI, Cheng C, Fan W, Dames C, Wu J, Minor AM (2014) Vanadium dioxide nanowire-based microthermometer for quantitative evaluation of electron beam heating. Nat Commun 5:4986

[8] Ghosh S, Bao W, Nika DL, Subrina S, Pokatilov EP, Lau CN, Balandin, AA (2010) Dimensional crossover of thermal transport in few-layer graphene. Nat Mater 9:555

[9] Taube A, Judek J, Lapinska A, Zdrojek M (2015) Temperature-dependent thermal properties of supported MoS2 monolayers. ACS Appl Mater Interfaces 7:5061-5065

[10] Iijima S, Ichihashi T (1986) Structural instability of ultrafine particles of metals. Phys Rev Lett 56:616

[11] Sun J, He L, Lo YC, Xu T, Bi H, Sun L, Zhang Z, Mao SX, Li J (2014) Liquid-like pseudoelasticity of sub-10-nm crystalline silver particles. Nat Mater 13:1007-1012

[12] Lai M, Kong Q, Bischak CG, Yu Y, Dou L, Eaton SW, Ginsberg, NS, Yang P (2017) Structural, optical, and electrical properties of phase-controlled cesium lead iodide nanowires. Nano Res 10:1107-1114

[13] Uskokovic V, Markovic S, Veselinovic L, Skapin S, Ignjatovic N, Uskokovic, DP (2018) Insights into the kinetics of thermally induced crystallization of amorphous calcium phosphate. Phys Chem Chem Phys 20:29221-29235

[14] Casu A, Lamberti A, Stassi S, Falqui A (2018) Crystallization of TiO2 nanotubes by in situ heating TEM. Nanomaterials 8:40

[15] Li P (2003) Electron irradiation damage to organic light-emitting materials. MSc thesis, University of Alberta, Canada

[16] Egerton RF, Li P, Malac M (2004) Radiation damage in the TEM and SEM. Micron 35:399-409

[17] Yokota T, Murayama M, Howe JM (2003) In situ transmission-electron-microscopy investigation of melting in submicron Al-Si alloy particles under electron-beam irradiation. Phys Rev Lett 91:265504

[18] Asoro MA, Kovar D, Ferreira PJ (2013) In situ transmission electron microscopy observations of sublimation in silver nanoparticles. Acs Nano 7:7844-52

[19] Shanley ES, Ennis JL (1991) The chemistry and free energy of formation of silver nitride. Ind Eng Chem Res 30:2503-2506.

[20] Paul KK, Ghosh R, Giri PK (2016) Mechanism of strong visible light photocatalysis by Ag2O-nanoparticle-decorated monoclinic TiO2 (B) porous nanorods. Nanotechnology 27: 315703

[21] Lian R, Yu H, He L, Zhang L, Zhou Y, Bu X, Xu T, Sun, L (2016) Sublimation of Ag nanocrystals and their wetting behaviors with graphene and carbon nanotubes. Carbon 101:368-376

[22] Suleiman MS, Joubert DP (2015) Theoretical calculations on the structural, electronic, and optical properties of bulk silver nitrides. Phys Status Solidi B 252: 2840-2852

[23] Yu R, Zhang XF (2005) Family of noble metal nitrides: First principles calculations of the elastic stability. Phys Rev B 72:054103

[24] Radnoczi G, Bokanyi E, Erdelyi Z, Misjak F (2017) Size dependent spinodal decomposition in Cu-Ag nanoparticles. Acta Mater 123:82-89

[25] Liu LC, Risbud SH (1994) Real-time hot-stage high-voltage transmission electron microscopy precipitation of CdS nanocrystals in glasses: Experiment and theoretical analysis. J Appl Phys 76:4576-4580

[26] Setyawan W, Cooper MW, Roche KJ, Kurtz RJ, Uberuaga BP, Andersson DA, Wirth BD (2018) Atomistic model of xenon gas bubble re-solution rate due to thermal spike in uranium oxide. J Appl Phys 124:075107

[27] Rath H, Dash BN, Benyagoub A, Mishra NC (2018) Sensitivity of Anatase and Rutile Phases of TiO2 to ion irradiation: Examination of the applicability of Coulomb Explosion and Thermal Spike Models. Sci Rep 8:1-12

[28] Mortazavi B, Cuniberti G, Rabczuk T (2015) Mechanical properties and thermal conductivity of graphitic carbon nitride: A molecular dynamics study. Comput Mater Sci 99:285-289

[29] Balandin AA (2011) Thermal properties of graphene and nanostructured carbon materials. Nat Mater 10:569

Figures

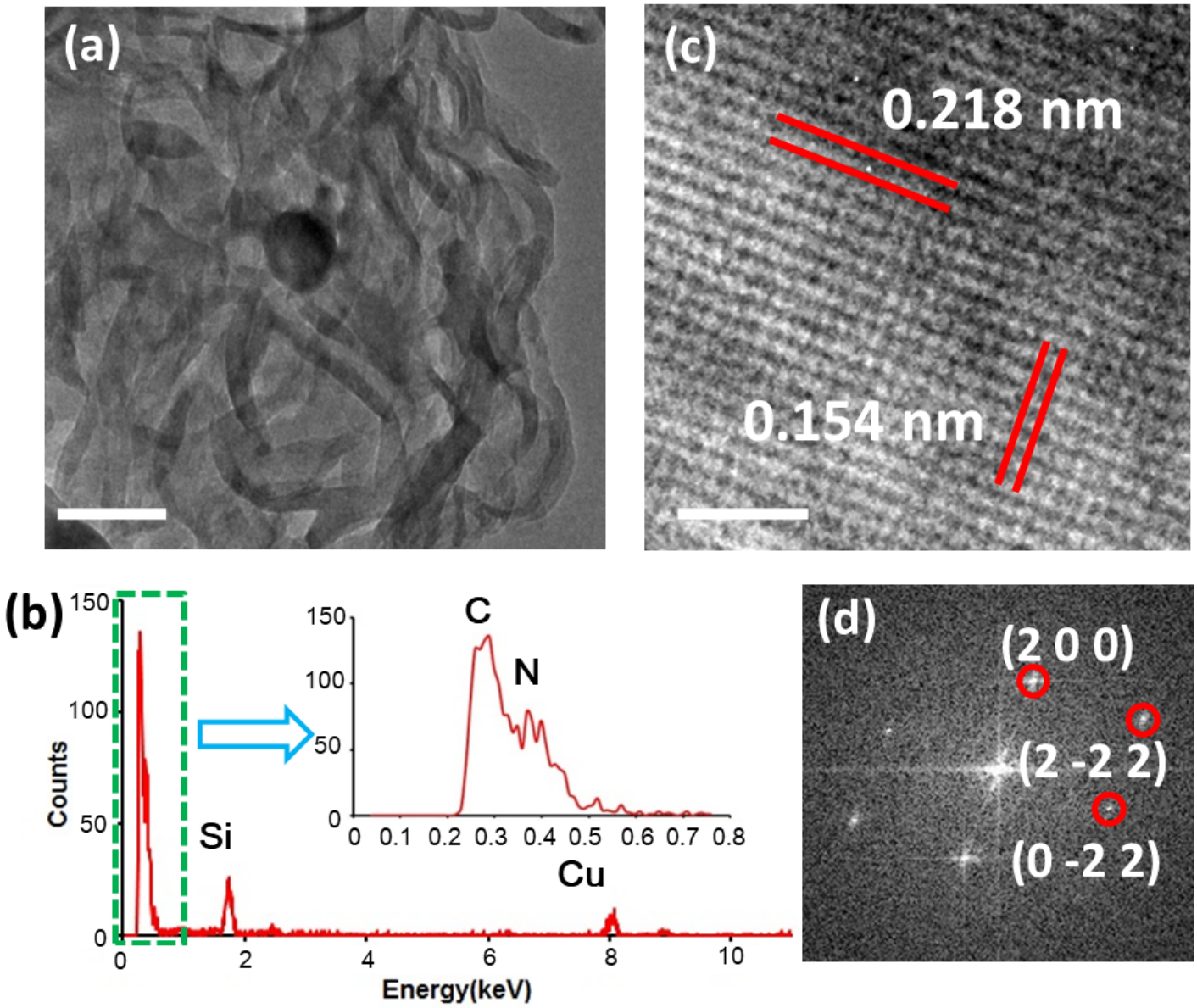

Figure 1

(a) Ag3N nanoparticles located in the g-C3N4 films (scale bar: 50nm); (b) EDX spectrum of the g-C3N4 film; (c) High-resolution TEM image of a Ag3N nanoparticle (scale bar: 1nm); (d) Fast Fourier transform pattern of the crystalline structure in (c).

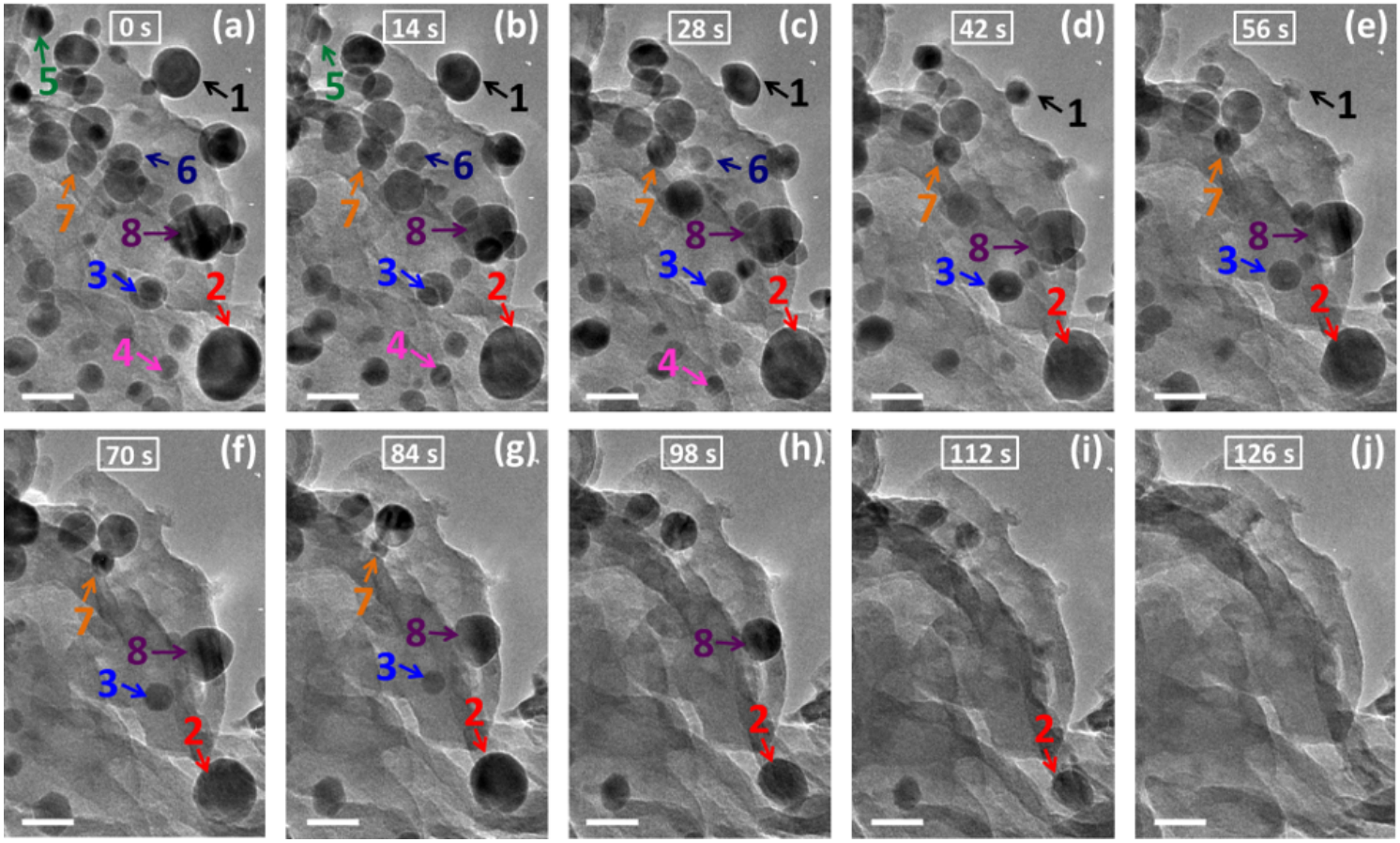

Figure 2

(a)-(j) The decomposition process of Ag3N nanoparticles inside g-C3N4 network under an beam irradiation with an intensity of 1.6×104A/m2 (scale bar:20nm)

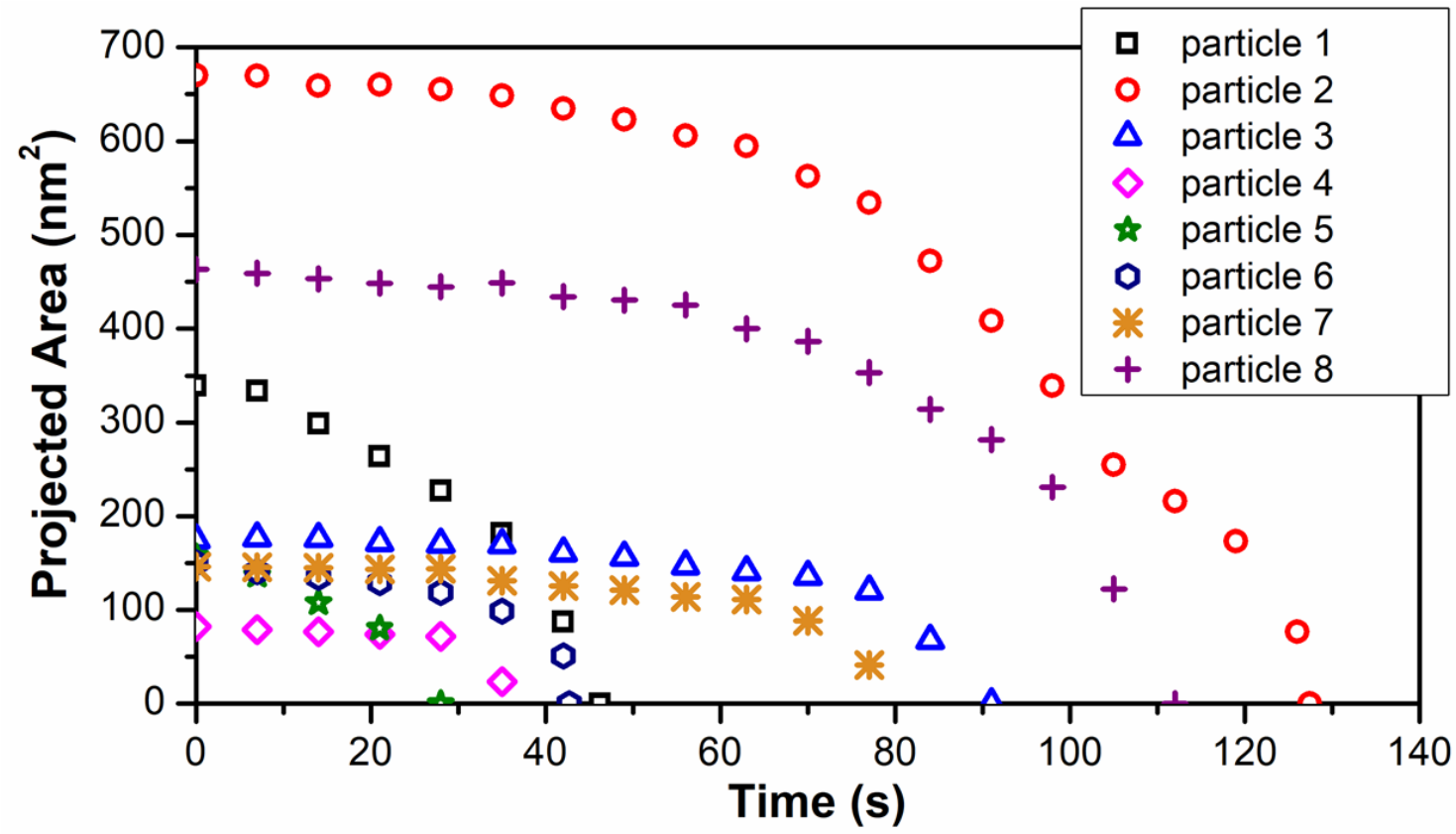

Figure 3

Recorded projected area change of selected eight Ag3N nanoparticles with irradiation time

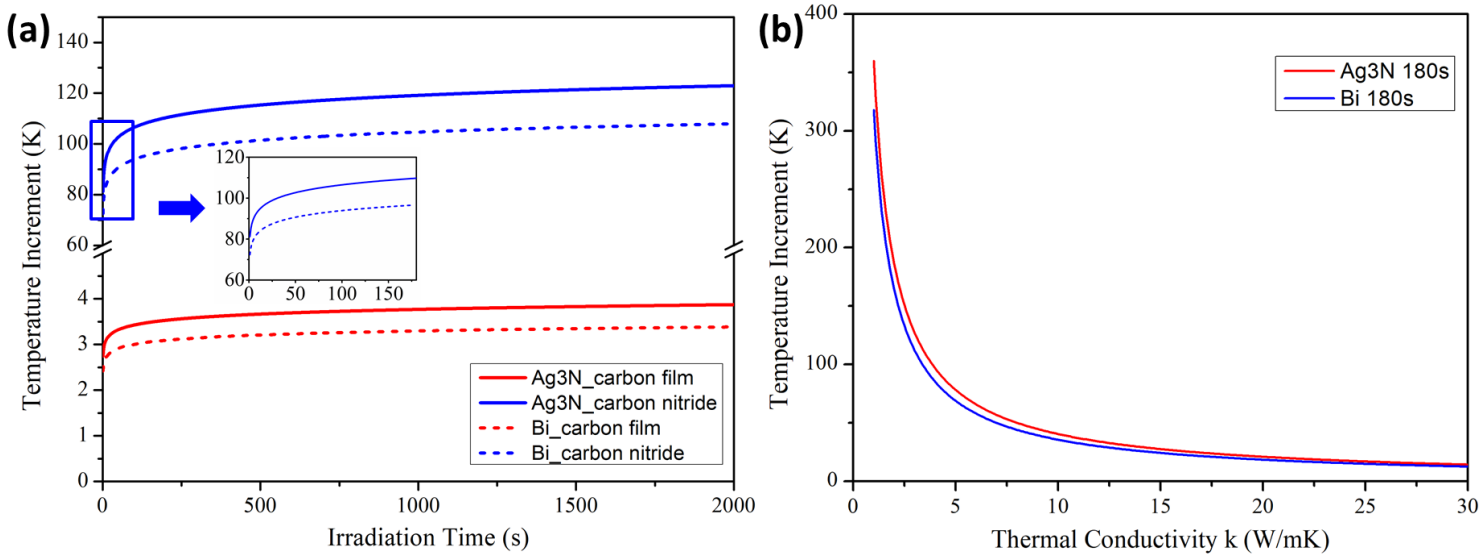

Figure 4

Semi-quantitative calculation results of (a) temperature increment with irradiation time for Ag3N and Bi nanoparticle in the g-C3N4 and holey carbon film network, respectively; (b) temperature increment of Ag3N and Bi nanoparticles in network having different thermal conductivity after 180s beam irradiation (all the beam intensity is 1.6×104A/m2)

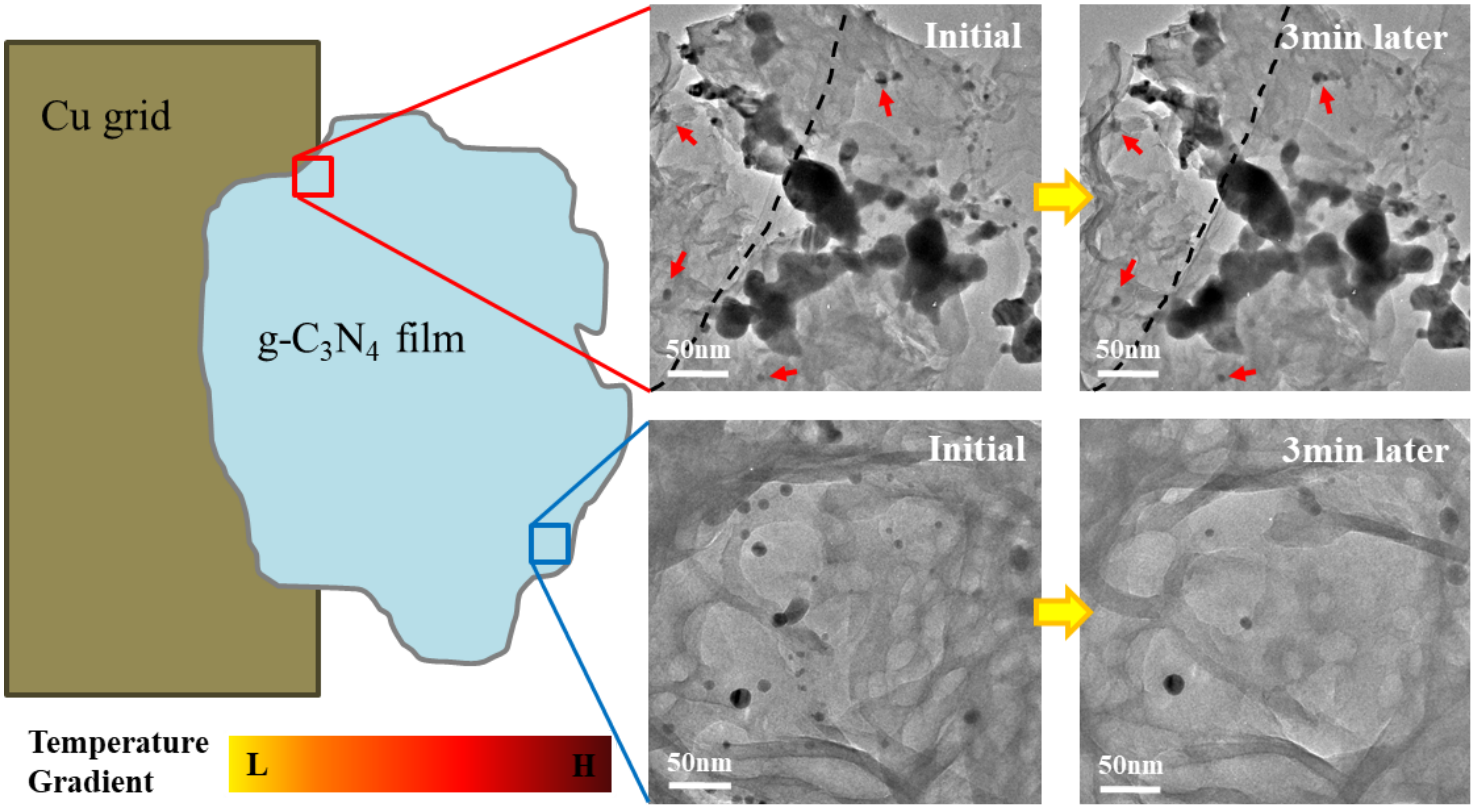

Figure 5

Temperature gradients in g-C3N4 films. Discrepant decomposition behaviors of Ag3N nanoparticles in a single-end fixed Ag3N-decorated-g-C3N4 sample. The conservation and disappearance of Ag3N nanoparticles in the regions nearby and far away from the Cu grid, respectively, suggest a strong temperature gradient.

Supplementary Files

This is a list of supplementary files associated with this preprint. Click to download.

- SupplementaryMaterial.docx